

MUM: flexible precise Monte Carlo code for muon propagation through thick layers of matter

Igor A. Sokalski, Edgar V. Bugaev, Sergey I. Klimushin

Institute for Nuclear Research, Russian Academy of Science, 60th October Anniversary prospect 7a, Moscow 117312, Russia
(December 2, 2024)

Theoretical and experimental progress of last years makes new demands to Monte Carlo algorithms for muon transportation through thick layers of matter. Here we present a new muon propagation code MUM (MUons+Medium) which possesses some advantages in accuracy and flexibility over analogous simulation codes presently in use. The code has been developed for the Baikal deep underwater experiment but we think it to be useful also for other experiments with natural fluxes of high energy muons and neutrinos. Basic concept of the code is described. The most important features of algorithm are briefly discussed. Selected results obtained with MUM are given and compared with ones from other codes. Results on the test for accuracy of treatment of muon energy losses with MUM are presented and analysed. It is evaluated to be of 2×10^{-3} or better, depending upon simulation parameters.

PACS number(s): 13.85Tp, 96.40.Tv, 02.70Lq

I. INTRODUCTION

Muon propagation through thick layers of matter was in the scope of interest for a long time since the first underground experiments with natural muon and neutrino fluxes had started. Development of “underground” technique has led to creation of number of underground, underwater and underice detectors by which a wide spectrum of problems is presently under investigation. Accurate calculation of muon transport plays an important role for such experiments because (a) atmospheric muons represent principal background for weak neutrino signal; (b) they are, at the same time, the only natural calibration source which allows to compare experimental and expected detector response and confirm correctness of the detector model and track reconstruction algorithm; (c) atmospheric muons are an object for investigation themselves and (d) neutrinos are commonly detected by muons which are born in νN interactions and propagate a distance in medium before are detected.

Along with analytical and semi-analytical methods (Refs. [1–13]) one widely uses Monte Carlo (MC) technique (Refs. [14–25]) to propagate muons through matter. There are several MC muon transportation codes currently in use (see Ref. [26] for detailed analysis of their advantages and disadvantages), but essential theoretical and experimental progress of last years makes to create new algorithms which take into account the most recent parametrizations for muon cross sections and use more accurate simulation technique. Besides, an “ideal” code must be flexible enough, i.e., for instance, be easily tuned for each concrete purpose to desirable equilibrium between accuracy, computation time and statistical error (note that for this one needs to know both accuracy of algorithm itself and error which is caused by this or that setting of simulation parameters). Here in this paper we present the MC muon propagation code MUM (MUons+Medium) written in FORTRAN which possesses some advantages in accuracy and flexibility over analogous simulation codes (though it does not still contain some important features in its current version, e.g. it does not give the 3D information about angular and lateral deviations of muons). The code has been developed for the Baikal deep underwater experiment (Ref. [27]) but we hope that it may be useful also for other experiments with natural fluxes of high energy muons and neutrinos.

We briefly describe the basic concept and main features of the code in Sec. II. Sec. III gives analysis for the algorithm accuracy. Sec. IV presents selected results of MUM which are compared with ones from other muon propagation MC codes, namely PROPMU (Ref. [22]) and MUSIC (Ref. [24]) (we used PROPMU version 2.01 and MUSIC version dated by April, 1999). Sec. V gives general conclusions. We also present parametrizations for muon cross sections used in MUM in Appendix A and give proof of formula for free path between two muon interactions, as treated in our code, in Appendix B.

II. CODE DESCRIPTION

Basic concept of the MUM code is as follows.

- (a) The most recent results on muon cross sections are used in the code (see Appendix A).

- (b) The code does not use any preliminary computed data files as an input, all necessary tables are computed at the stage of initiation on the base of five relatively short routines, four of which compute differential cross sections $d\sigma(E, v)/dv$ (where E is muon energy, v is fraction of energy lost $v = \Delta E/E$) for bremsstrahlung, direct e^+e^- -pair production, photonuclear interaction and knock-on electron production, correspondingly, and fifth one computes ionization energy loss. Thus, it is easy to correct or even entirely change any parametrization according to new published improvements and/or user's taste.
- (c) We tried to decrease the "methodical" part of systematic error which originate from finite accuracy of the interpolation, numerical integration, etc., down to as low level as possible, special attention was put on simulation procedures for free path and fraction of energy lost.
- (d) The most important parameters (including material) are changeable and represent input parameters for initiation routine. They can be tuned to an optimum combination, depending upon desirable accuracy, necessary statistics and restriction on the computation time for each concrete problem.
- (e) Special efforts were directed to make the code to be as fast as possible.
- (f) The code combines algorithms for transportation of muons through thick layers of matter down to detector and for simulation muon interactions within detector sensitive volume. This is important for deep underwater/ice Cherenkov neutrino telescopes (see Refs. [27-30]), where the same medium is used as shield which absorbs atmospheric muons and as detecting medium in which muons and shower particles resulting from muon interactions generate Cherenkov photons detected by phototubes.

In order to get finite computation time muon energy losses are decomposed into two parts: "stochastic" loss (SEL) with relatively large energies transferred either to the real or virtual photon or to knock-on electron and "continuous" loss (CEL) with relatively small energy lost. We use two different criteria by which the given muon interaction is attributed either to SEL or to CEL. The first one (relative) is for the case when muon is transported down to detector location: interaction belongs to SEL if fraction of energy lost, $v = \Delta E/E$, is more than v_{cut} ($v \geq v_{cut}$) and to CEL, if $v < v_{cut}$. Second, absolute criterium, is usefull when simulating muon interactions within underwater/ice arrays to obtain the detector response with the fixed energy threshold: interaction is of SEL type if $\Delta E \geq \Delta E_{cut}$ and of CEL type, if $\Delta E < \Delta E_{cut}$.

SEL is treated by direct simulation of $v \geq v_{cut}$ or $v \geq \Delta E_{cut}/E$ for each single interaction according to shape of differential cross sections $d\sigma(E, v)/dv$ for bremsstrahlung, direct e^+e^- -pair production, photonuclear interaction and knock-on electron production. For composed materials like water differential cross sections are computed as:

$$\frac{d\sigma^j}{dv}(E, v) = \sum_{i=1}^n k_i \frac{d\sigma_i^j}{dv}(E, v), \quad (2.1)$$

where j indicates type of interaction; i runs over n kinds of atoms, given material consists of; $k_i = N_i/N_{tot}$ is fraction of i -th element; N_i and N_{tot} are number of given kind of atoms and total number of atoms, respectively, per unit of material volume. Notice that for a single material like standard rock Eq. (2.1) (as well as other general expressions below) is still valid but becomes simplified with $n = 1$ and $k_1 = 1$. Type of interaction is simulated according to proportion between total cross sections

$$\sigma^\gamma : \sigma^{e^+e^-} : \sigma^{pn} : \sigma^\delta \quad (2.2)$$

(upper indexes γ , e^+e^- , pn and δ stand for bremsstrahlung, e^+e^- -pair, photonuclear interaction and knock-on electrons, respectively), which are computed by:

$$\sigma^j = \sum_{i=1}^n \left[k_i \int_{v_{cut}}^{v_{max}^{i,j}} \frac{d\sigma_i^j(E, v)}{dv} dv \right], \quad (2.3)$$

where $v_{max}^{i,j}$ is maximum kinematically allowed fraction of energy lost for i -th element at j -th kind of interaction.

CEL is calculated by formula:

$$\left[\frac{dE}{dx}(E) \right]_{CEL} = \frac{N_A}{A_{eff}} \rho E \sum_j \sum_{i=1}^n \left[k_i \int_{v_{min}^{i,j}}^{v_{cut}} \frac{d\sigma_i^j(E, v)}{dv} v dv \right]$$

$$\begin{aligned}
& + \left[\frac{dE}{dx}(E) \right]_{B-B} \\
& - \frac{N_A}{A_{eff}} \rho E \sum_{i=1}^n \left[k_i \int_{v_{cut}}^{v_{max}^{i,\delta}} \frac{d\sigma_i^\delta(E, v)}{dv} v dv \right].
\end{aligned} \tag{2.4}$$

Here j in the first term runs over three radiative processes only (bremsstrahlung, e^+e^- -pair production and photonuclear interaction); N_A is the Avogadro number; ρ is material density; $A_{eff} = N_{tot}^{-1} \sum_{i=1}^n (N_i A_i)$ is an effective atomic weight for given material; A_i is atomic weight for i -th element; $[dE(E)/dx]_{B-B}$ is ionization energy loss calculated by Bethe-Bloch formula with corrections for density effect (see Appendix A 5); $v_{min}^{i,j}$ is minimum kinematically allowed fraction of energy lost for i -th element at j -th process. Parametrizations of muon cross sections, as used in MUM are given in Appendix A.

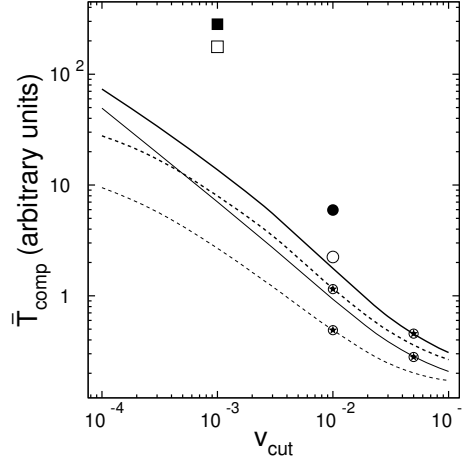


FIG. 1. Averaged computation time \bar{T}_{comp} which is necessary for muon propagation in pure water vs. v_{cut} , as obtained with the MUM code. Thick lines correspond to muon with initial energy $E_s = 9$ TeV transported down to $D = 10$ km. Thin lines are for $E_s = 1$ TeV and $D = 3$ km. Solid lines show results for ionization included in SEL, dashed ones correspond to entirely “continuous” ionization. Circled asterisks on curves correspond to evaluated limit of the MUM code accuracy which is equal to $v_{cut} \sim 0.05$ if ionization is included in SEL and to $v_{cut} \sim 0.01$ if ionization is entirely “continuous”. It is not recommended to set v_{cut} to larger values in the MUM code (see Sec. III). Circles and squares show values for \bar{T}_{comp} , as obtained with muon propagation codes PROPMU (Ref. [22]) and MUSIC (Ref. [24]), correspondingly. Closed markers are for $E_s = 9$ TeV and $D = 10$ km, open ones are for $E_s = 1$ TeV and $D = 3$ km. Notice that both PROPMU and MUSIC are three-dimensional codes (in contrast to presented version of MUM).

Replacement $v_{cut} \rightarrow \Delta E_{cut}/E$ in Eqs. (2.3) and (2.4) allows to compute corresponding values also for “absolute” treatment of the boundary between CEL and SEL. Formulae (2.1), (2.3) and (2.4) are tabulated in both definitions of energy loss decomposition during initiation of the code. These tables are then referenced during execution of simulation routines. v_{cut} and ΔE_{cut} represent parameters for MUM initiation procedure and can be set to $10^{-4} \leq v_{cut} \leq 0.2$ and $10 \text{ MeV} \leq \Delta E_{cut} \leq 500 \text{ MeV}$, correspondingly. Note, that even little increase of v_{cut} and ΔE_{cut} leads to significant advantage for computation time because of extremely steep dependence of muon cross sections upon v , but it also results in some loss of simulation accuracy. Optionally, cross section for knock-on electron production $d\sigma^\delta(E, v)/dv$ can be set to zero for “relative” decomposition energy loss into CEL and SEL. In the last case muon propagation down to detector is simulated with entirely “continuous” ionization and its fluctuations are neglected (but simulation of the muon interactions with fixed energy threshold includes fluctuations in ionization loss in any case). It results in immaterial (for most purposes) loss of accuracy but computation time decreases by a factor of ~ 2 . We have investigated in details how simplified “continuous” treatment of ionization, value of v_{cut} and some other parameters influence upon simulation accuracy. Results are reported in separate paper (Ref. [31]). Here in Fig. 1 we only show dependence of computation time on v_{cut} and model for ionization energy loss, as was obtained with the MUM code. Data for muon transportation codes PROPMU (Ref. [22]) and MUSIC (Ref. [24]) are given on the figure, as well. We must emphasize that data on computation time for other codes are shown only for reference. In contrast to presented version of MUM, both PROPMU and MUSIC are three-dimensional codes (PROPMU treats only Coulomb multiple scattering while in MUSIC the angle of the muon acquired in all radiative processes is also simulated) which takes additional time but gives more information at the output.

The principal steps of simulation algorithm are as follows. First, for muon with initial energy E_1 the free path L till interaction is simulated. We would like to stress that an accurate technique is used at this step in the MUM code in order to take into account dependence of muon cross sections upon energy which is often neglected. After random number η uniformly distributed in a range from 0 to 1 has been simulated, the following set of equations is solved:

$$\begin{cases} -\ln(\eta) = \int_{E_2}^{E_1} [(dE(E)/dx)_{CEL} \bar{L}(E)]^{-1} dE \\ L = \int_{E_2}^{E_1} [(dE(E)/dx)_{CEL}]^{-1} dE \end{cases} \quad (2.5)$$

(proof of (2.5) is given in Appendix B). Here, $E_2 < E_1$ is muon energy at the point of interaction, $(dE(E)/dx)_{CEL}$ is determined by (2.4), and energy dependent mean free path $\bar{L}(E)$ between two sequential interactions with fraction of energy lost $v \geq v_{cut} = \Delta E_{cut}/E$ is expressed by

$$\bar{L}(E) = \frac{A_{eff}}{\rho N_A} \left\{ \sum_j \sum_{i=1}^n \left[k_i \int_{v_{cut}}^{v_{max}^{i,j}} \frac{d\sigma_i^j(E, v)}{dv} dv \right] \right\}^{-1}. \quad (2.6)$$

First equation in (2.5) is solved for variable E_2 , next free path L can be found by second equation (actually, in order to avoid lost of computation time, functions $E_2(E_1, \eta)$, $L(E_1, E_2)$ (2.5) and $\bar{L}(E)$ (2.6) are tabulated in advance during MUM initiation). Fig. 2 shows what error is avoided by this method. Upper plot shows function $\bar{L}(E)$ for pure water. Two sets of curves are presented for two models of ionization. Each set includes dependencies for 3 values of v_{cut} : 10^{-4} , 10^{-3} and 10^{-2} . In fact, $\bar{L}(E)$ is almost a constant for $E > 5$ TeV but changes steeply below this energy threshold. It increases with decrease of energy if ionization is entirely “continuous” and, on the contrary, it decreases if ionization is included in SEL. Thus, if one computes free path just as $L = -\bar{L}(E_1) \ln(\eta)$ neglecting energy dependence of muon cross sections one overestimates free path (and, consequently, underestimates SEL) in the case when ionization is included in SEL and, on the contrary, one underestimates free path (and overestimates SEL) in the case of completely “continuous” ionization. Lower plot of Fig. 2 shows resulting error in the value of real free path if $-\ln(\eta) = 1$ (for larger $-\ln(\eta)$ the effect is more significant). The set of curves represent dependencies k vs. muon energy E where $k = \bar{L}(E)/L$ with $\bar{L}(E)$ computed by (2.6) and L obtained from (2.5). For correct treatment of ionization the error is of positive sign and does not exceed 1 % if $v_{cut} \leq 10^{-3}$. But it reaches 10–15 % for $v_{cut} = 10^{-2}$ which leads to 1-2% underestimation of total energy loss below muon energy 1 TeV. As was shown in Ref. [31] such error may distort results of simulation noticeable. For the case with “continuous” ionization the error is of negative sign and, again, is more significant for large v_{cut} which leads to overestimation of energy loss. After the free path L is simulated, the type of interaction and fraction of energy lost $v = \Delta E/E_2$ are simulated according to (2.2) and (2.1), correspondingly, new muon energy $E'_1 = E_2 - \Delta E$ is determined and all these steps are repeated sequentially until muon either stops or reaches the level of observation.

We close this section with several remarks related to important details of described algorithm.

- We set the lower threshold muon energy $E_t = 0.16$ GeV (which corresponds to the Cherenkov threshold for muon in water). If at some step of procedure muon energy becomes $E < E_t$ the muon is considered as stopped.
- At any settings of input parameters our algorithm treats muon energy loss as entirely “continuous” if $E < 10$ GeV.
- Formally, initial muon energies in the interval $10 \text{ GeV} \leq E \leq 1 \text{ EeV}$ can be processed by the MUM code. But actually, uncertainties with muon cross sections (especially, for photonuclear interaction) and influence of Landau-Pomeranchuk-Migdal effect, which is not taken into account in our algorithm, make one to use MUM with care for muon energies $E > 1 \text{ PeV}$.
- Besides muon transportation algorithm described above, the code includes number of routines which allows to obtain directly values for differential and total cross sections, mean free path, energy loss and other related data for given setting of input parameters, Also there are several test procedures which provide by data concerning accuracy of different operations, depth muon spectra, distribution of energy transfers, etc. (see Sec. III and Sec. IV for selected output of these procedures).
- We plan the further development of the MUM code in order to improve its accuracy and flexibility. In particular, it is planned to add a part which would treat the 3rd dimension to simulate angular deviation.

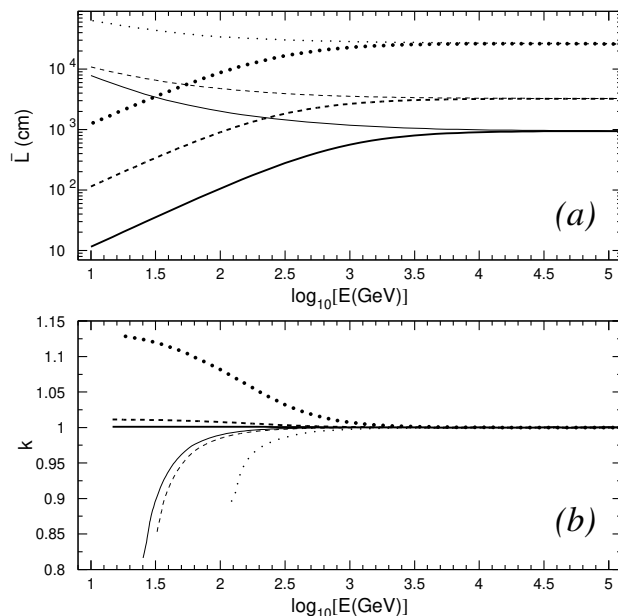


FIG. 2. (a) - dependence of mean free path \bar{L} (2.6) between two sequential interactions with fraction of energy lost $v > v_{cut}$ vs. muon energy E . Two sets of curves correspond to two models of ionization. Thick lines are for ionization included in SEL, thin ones correspond to entirely "continuous" ionization. Solid lines: $v_{cut} = 10^{-4}$; dashed lines: $v_{cut} = 10^{-3}$; dotted lines: $v_{cut} = 10^{-2}$.

(b) - resulting error k in the value of free path between two sequential interactions computed for $-\ln(\eta) = 1$. Curves represent dependencies $k = \bar{L}(E)/L$ with $\bar{L}(E)$ computed by Eq. (2.6) and L obtained from Eqs. (2.5) vs. muon energy E . Thickness and type of lines are of the same meaning as for plot (a). See text for more details.

III. ALGORITHM ACCURACY

Accuracy of muon propagation algorithm includes both "outer" uncertainty which results from uncertainties of used parametrizations for muon cross sections and "inner" accuracy which is caused by algorithm itself. Influence of "outer" uncertainties upon result of simulation was discussed in our Ref. [31]. Besides, this part of error sources can not be avoided when developing a muon transport algorithm, one can only try to use the most recent results on muon cross sections and to provide for eventuality to upgrade corresponding part of code as easily as possible, when necessary. Therefore, in this section we concentrate only on "inner" accuracy of the MUM code. Again, it can be divided into two parts, first of which depends upon model of simulation (value of v_{cut} , entirely "continuous" or included in SEL ionization energy loss, etc.) and was studied in details in Ref. [31]. Second part is determined by accuracy of integration, interpolation, simulation of single muon interaction and number of other procedures which any muon code consists of and which have to be performed to simulate muon propagation. Summarized accuracy of these procedures should be, in any case, not worse than "outer" uncertainty in muon cross sections and it is natural quality criterium for muon transport algorithm.

It is impossible, due to restricted size of article, to present all data which demonstrate the accuracy of each algorithm step. So, we include in this report only two figures which show summarized accuracy of the whole code. In Fig. 3 and Fig. 4 the relative difference $(L_s - L_i)/L_i$ between "simulated" L_s and "integrated" L_i total muon energy loss is presented as a function of muon energy for several values of v_{cut} and two models of ionization energy loss. Fig. 3 contains plots obtained for pure water, Fig. 4 presents data on standard rock ($\rho = 2.65 \text{ g cm}^{-3}$, $A = 22$, $Z = 11$). Values of L_s were obtained as follows. For given muon energy we selected a distance D which was as large as possible (in order to get enough statistics) but, at the same time, was short enough to be passed by muons without decrease their energy down to zero. Values of D were taken in the range from 0.5 m to 300 m depending upon muon energy, value of v_{cut} and medium. Then we simulated propagation of $N = 4 \times 10^6$ muons with given energy E_1 over distance D and for each i -th muon fixed its final energy E_2^i . After that "simulated" energy loss L_s was calculated as

$$L_s = \frac{1}{D} \left(E_1 - \frac{1}{N} \sum_{i=1}^N E_2^i \right). \quad (3.1)$$

L_i was computed as

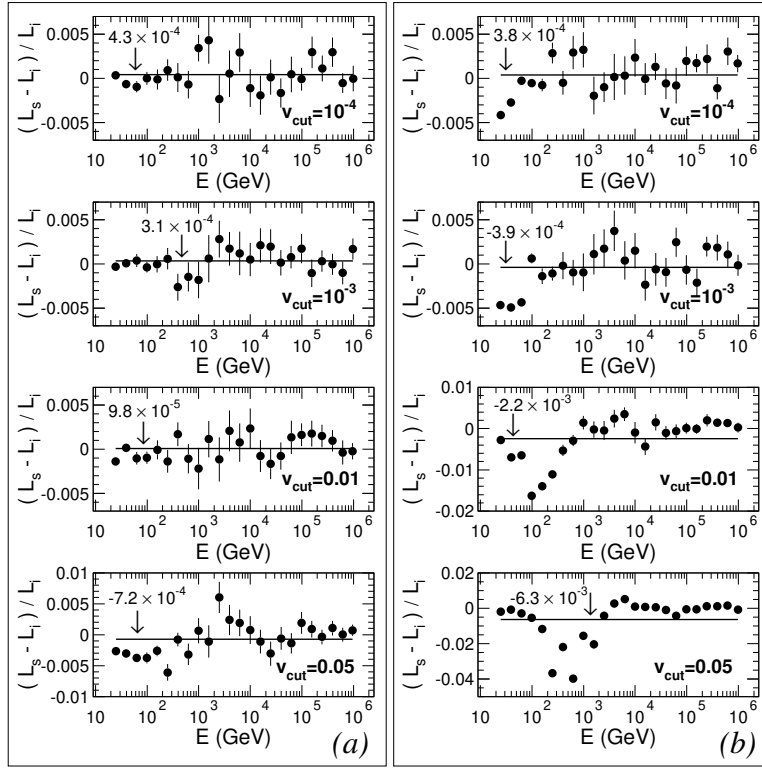


FIG. 3. Relative difference $(L_s - L_i)/L_i$ between “simulated” L_s (3.1) and “integrated” L_i (3.2), (3.3) total muon energy loss. Horizontal solid line on each plot shows averaged over 24 tested muon energies value for $(L_s - L_i)/L_i$ which, additionally, is given at the upper left corner by the figure. Statistical error at 1σ -level is shown at each point. (a) - ionization is included in SEL; (b) - ionization is entirely continuous.

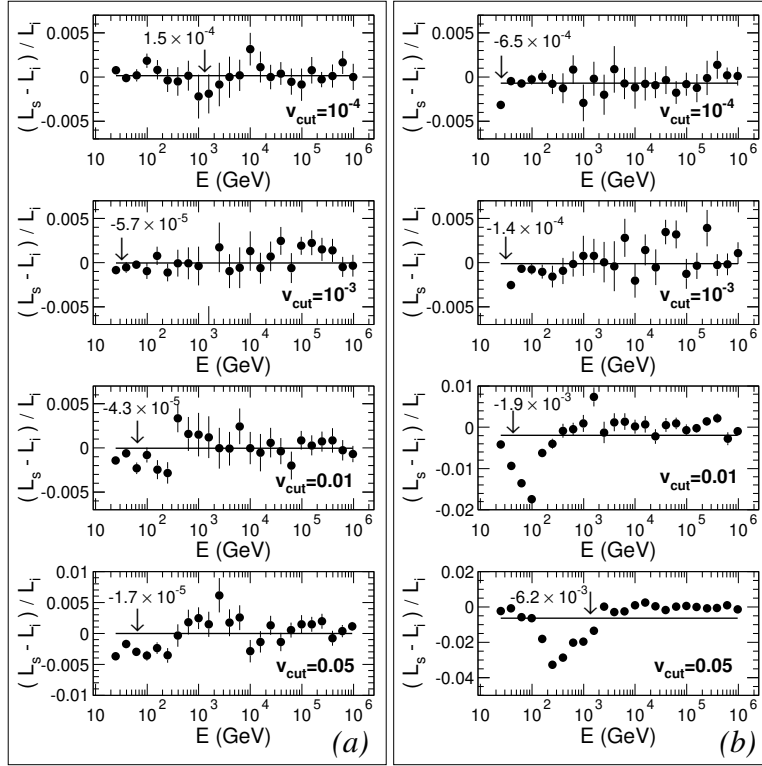


FIG. 4. The same as in Fig. 3 for standard rock ($\rho = 2.65 \text{ g cm}^{-3}$, $A = 22$, $Z = 11$).

$$L_i = \frac{1}{D}(E_1 - E_2), \quad (3.2)$$

where E_2 was found from expression

$$D = \int_{E_2}^{E_1} \left\{ \frac{N_A}{A_{eff}} \rho E \sum_j \sum_{i=1}^n \left[k_i \int_{v_{min}^{i,j}}^{v_{max}^{i,j}} \frac{d\sigma_i^j(E, v)}{dv} v dv \right] + \left[\frac{dE}{dx}(E) \right]_{B-B} \right\}^{-1} dE \quad (3.3)$$

(j runs over three radiative processes). Horizontal solid line on each plot shows the value for $(L_s - L_i)/L_i$ averaged over 24 tested muon energies which, additionally, is given at upper left corner by a figure. In our opinion, presented relative difference between L_i and L_s is a good accuracy criterium for the whole algorithm because errors from all procedures which treat both CEL and SEL parts of energy loss are collected and summarized in the value of L_s .

Fig. 3(a) and Fig. 4(a) indicate an excellent accuracy of the MUM code for ionization included in SEL and $v_{cut} \leq 10^{-2}$ both for water and standard rock. In fact, with the exception of several points on plots for $v_{cut} = 10^{-2}$ at relatively low muon energies $E \leq 100$ GeV, there are no statistically significant systematic deviations and averaged value of $(L_s - L_i)/L_i$ is in a range of $5 \times 10^{-5} - 5 \times 10^{-4}$. Some noticeable systematics (which is of the same type for both tested materials) appears on plots for $v_{cut} = 5 \times 10^{-2}$ but all points here are still within only 0.6%-deviations which, besides, are of both signs, so averaged accuracy remains within 10^{-3} . Fig. 3(b) and Fig. 4(b) (which correspond to completely continuous ionization) shows somewhat worse “inner” accuracy of the code, which, again, falls down when v_{cut} increases. Statistically significant likeness of plots obtained for water and standard rock can be seen also. Accuracy is indicated within 10^{-2} (with except for 4 points around muon energy $E = 100$ GeV) up to $v_{cut} = 10^{-2}$ with averaged accuracy within 2×10^{-3} . This last value may be used as a quantitative evaluation of accuracy for the MUM code.

Thus, we conclude that if using an optimistic evaluation of 1% for uncertainties in muon cross sections (Ref. [26,32]) our algorithm does not contribute the “inner” error which would exceed “outer” one for any $v_{cut} \leq 5 \times 10^{-2}$ (if ionization is included in SEL) and for any $v_{cut} \leq 10^{-2}$ (if ionization is treated as entirely “continuous process”), independently upon material. These combinations of v_{cut} and model for ionization energy loss themselves were shown in Ref. [31] to be quite acceptable when simulating muon depth flux intensity and/or spectra. This allows us to contend that our algorithm gives reliable results, i.e. “inner” accuracy is better comparing with “outer” one, for depth muon fluxes and spectra with settings of parameters pointed out. Note that from the point of view of computation time it is always more advantageous to use model of completely “continuous” ionization and set v_{cut} to large value (see Fig. 1). For some special methodical purposes (e.g., investigation of behaviour of survival probabilities depending of material composition) it can be necessary to include ionization in SEL and set v_{cut} to finer values down to $v_{cut} = 10^{-3}$ (see Fig. 1 in Ref. [31]). On the other hand, less fine but faster tuning can be used for test runs. It is impossible to foresee each possible application, but we hope that analysis presented in Ref. [31] and in this section will help to tune the MUM code correctly to each concrete case. Moreover, MUM is provided with a special test routine which produces at output data on dependence of $(L_s - L_i)/L_i$ upon muon energy for the given setting of input parameters. This allows to evaluate and know accuracy of simulation.

IV. SELECTED RESULTS AND COMPARISON WITH OTHER CODES

Fig. 5 shows energy distributions which results from direct simulation with the MUM code. Muons were sampled according to sea-level vertical muon spectrum proposed in Ref. [33] and propagated down to depths 1 km w.e., 3 km w.e. and 10 km w.e. in pure water (Fig. 5(a)) and in standard rock (Fig. 5(b)). For each distribution simulation continued until 10^4 muons with energy $E \geq 0.16$ GeV had been detected at the level of observation. In the case of pure water the mean energies are equal to $\bar{E} = 148 \pm 2$ GeV, 330 ± 5 GeV and 539 ± 10 GeV at depths $D = 1$ km w.e., 3 km w.e. and 10 km w.e., respectively (figures are accompanied with statistical errors at 1σ -level). Corresponding values for standard rock are $\bar{E} = 123 \pm 2$ GeV, 256 ± 4 GeV and 387 ± 7 GeV which is in a good agreement with mean energies computed for standard rock with the MUSIC code (Ref. [24]), which are $\bar{E} = 125 \pm 1$ GeV, 259 ± 3 GeV and 364 ± 4 GeV, respectively. Note that differences in mean energies \bar{E} are caused not only by codes themselves but also by different sea-level muon spectra used to obtain depth energy distributions (we used spectrum from Ref. [33], authors of Ref. [24] obtained their results with Gaisser spectrum from Ref. [34]). More data from MUM on depth muon spectra can be found in Ref. [33].

Fig. 6 shows muon spectra resulted from monoenergetic muon beam with initial energies $E_s = 1$ TeV (Fig. 6(a)), $E_s = 9$ TeV (Fig. 6(b)) and $E_s = 1$ PeV (Fig. 6(c)) after propagation of distances 3 km, 10 km and 40 km in pure water, correspondingly, as simulated with codes MUM, MUSIC and PROPMU. Again, an excellent agreement is observed

between MUM's and MUSIC's data, while data obtained with PROPMU indicates an essential difference. Survival probabilities (fraction of muons which survive after propagation of corresponding depth) for displayed plots are as follows: $p(1 \text{ TeV}, 3 \text{ km}) = 0.029$ (MUM), 0.033 (MUSIC), 0.19 (PROPMU); $p(9 \text{ TeV}, 10 \text{ km}) = 0.030$ (MUM), 0.031 (MUSIC), 0.048 (PROPMU); $p(1 \text{ PeV}, 40 \text{ km}) = 0.078$ (MUM), 0.084 (MUSIC), 0.044 (PROPMU).

The last figure of this section (Fig. 7) shows survival probabilities versus distance of propagation D in pure water as computed with our code MUM, MUSIC and PROPMU for a set of initial muon beam energies E_s from $E_s = 500 \text{ GeV}$ to $E_s = 30 \text{ PeV}$. At simulations of data presented on the Fig. 7 muons are treated as stopped as soon as their energy decreases down to “cut-off” energy $E = 10 \text{ GeV}$. No statistically significant difference is visible between survival probabilities resulting from simulation with MUM and MUSIC but survival probabilities computed with the PROPMU code are noticeably higher (up to factor 6) at muon energies $E \leq 30 \text{ TeV}$ and become less at $E \geq 30 \text{ TeV}$. We suppose that the main reason for these differences is that MUM and MUSIC use more or less similar parametrizations for muon cross sections which contain improvements done for last 10 years which passed after PROPMU had been written. Also “inner” accuracy of each of three compared codes may contribute to disagreement but we can not evaluate this contribution because we do not know “inner” accuracy both for MUSIC and PROPMU.

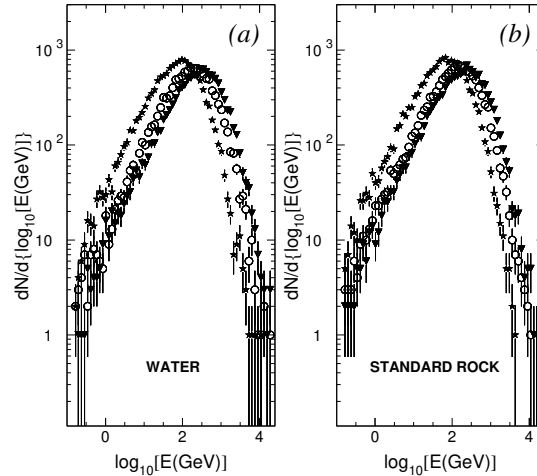


FIG. 5. Energy distributions for vertical muons sampled according to sea-level spectrum from Ref. [33] after propagation down to depths $D = 1 \text{ km}$ w.e. (asterisks), $D = 3 \text{ km}$ w.e. (circles), $D = 10 \text{ km}$ w.e. (triangles) as simulated with the MUM code for pure water (a) and standard rock (b). For each distribution simulation continued until 10^4 muons with energy $E \geq 0.16 \text{ GeV}$ had been detected at the level of observation.

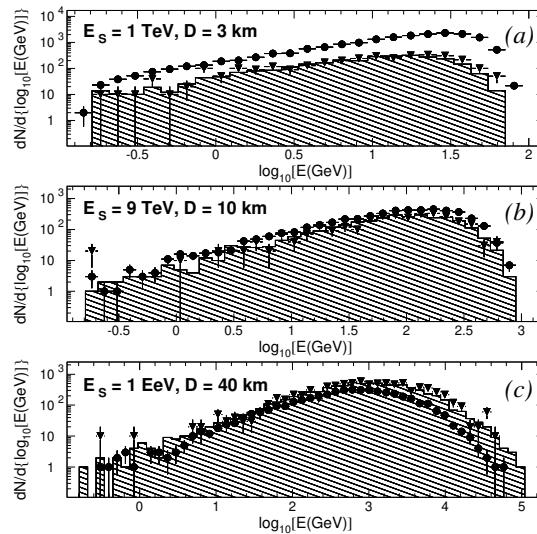


FIG. 6. Muon spectra resulting from monoenergetic muon beam with initial energy $E_s = 1 \text{ TeV}$ (a), $E_s = 9 \text{ TeV}$ (b) and $E_s = 1 \text{ EeV}$ (c) after propagation down to depths $D = 3 \text{ km}$, 10 km and 40 km of pure water, correspondingly, as simulated with muon transportation codes MUM (histograms), PROPMU (Ref. [22], circles) and MUSIC (Ref. [24], triangles). Corresponding values for survival probabilities p (fraction of muons survived after propagation) are equal to: $p(1 \text{ TeV}, 3 \text{ km}) = 0.029$ (MUM), 0.033 (MUSIC), 0.19 (PROPMU); $p(9 \text{ TeV}, 10 \text{ km}) = 0.030$ (MUM), 0.031 (MUSIC), 0.048 (PROPMU); $p(1 \text{ PeV}, 40 \text{ km}) = 0.078$ (MUM), 0.084 (MUSIC), 0.044 (PROPMU).

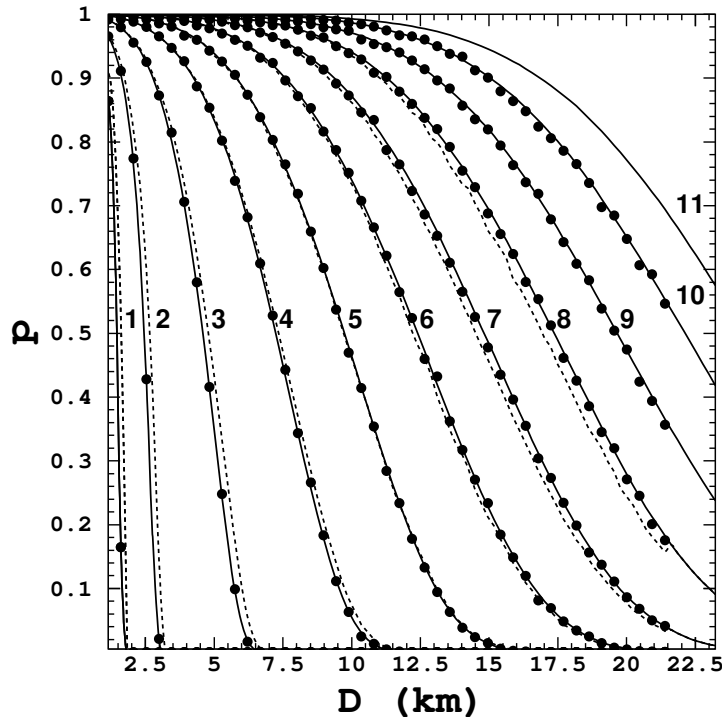


FIG. 7. Survival probabilities versus distance of propagation D in pure water as computed with the codes MUM (solid lines), MUSIC (circles) and PROPMU (dashed lines). Figures near curves indicate initial energy of muon beam E_s . The set of E_s for given plot is as follows: 500 GeV (1), 1 TeV (2), 3 TeV (3), 10 TeV (4), 30 TeV (5), 100 TeV (6), 300 TeV (7), 1 PeV (8), 3 PeV (9), 10 PeV (10), 30 PeV (11). At simulations of data presented on the plot muons are treated as stopped as soon as their energy decreases down to “cut-off” energy $E = 10$ GeV.

V. CONCLUSIONS

We have presented the muon propagation Monte Carlo code MUM (MUons+Medium) and have given selected results obtained with the code for depth muon spectra and survival probabilities in comparison with results obtained with other muon transportation codes.

Our own point of view on advantages of MUM is as follows. It is flexible enough and provides with eventuality to tune parameters of simulation to an optimum for each concrete case to get desirable equilibrium between computation time and accuracy. Besides, medium composition and parametrizations for muon cross sections are easily changeable. “Inner” accuracy of the code is high enough and is evaluated by us to be 2×10^{-3} or better if $v_{cut} \leq 0.05$ (for ionization included in SEL) or $v_{cut} \leq 0.01$ (if ionization is entirely “continuous”). Dependence of accuracy upon simulation parameters (v_{cut} , model for ionization, medium, etc.) was investigated in details and reported in this article and in Ref. [31]. In addition, MUM provides with the special routine which allows to test “inner” accuracy for each set of simulation parameters and take it into account when evaluating significance of results. “Outer” accuracy (caused by uncertainties of parametrizations for muon cross sections) is also high enough because the most recent improvements for cross sections are used and, as said above, new further improvements can be taken into account easily. Also computation time in MUM have been decreased down to low level which allows to get statistically significant results in the most practical applications for relatively short time.

The main disadvantage is that our algorithm does not still treat the three dimensions in current version like, e.g., PROPMU and MUSIC codes. So, it can not be used to obtain lateral and angular deviations of muons at propagation through matter. Also other important features are still missed in MUM - for instance, treatment of composed medium as it is possible in the latest version of the MUSIC code (Ref. [35]).

But we consider the current version of MUM as a basis for further development and plan to complement it, step by step, by all necessary features.

The MUM code is available on request to sokalski@pcbai10.inr.ruhep.ru.

ACKNOWLEDGMENTS

We would like to express our gratitude to I. Belolaptikov for number of useful advices which allowed to improve the MUM code essentially. We are grateful to A. Butkevich, R. Kokoulin, V. Kudryavzev, P. Lipari, W. Lohmann, V. Naumov, O. Streicher and Ch. Wiebusch who read the paper at the draft study and gave their comments which mostly were taken into account both in the final version of the article and in the code itself. One of us (I.S.) was benefited a lot by attention and support of L. Bezrukov and Ch. Spiering.

APPENDIX A: PARAMETRIZATIONS FOR MUON CROSS SECTIONS USED IN THE MUM CODE

We use the following designations in this section: $\alpha = 7.297353 \times 10^{-3}$ – fine structure constant; $r_e = 2.817941 \times 10^{-13}$ cm – classical radii of electron; $m_\mu = 0.1056593$ GeV and $m_e = 0.5110034$ MeV – muon and electron masses, correspondingly; $N_A = 6.022 \times 10^{23}$ – the Avogadro number; Z and A – electric charge and atomic weight, correspondingly; $e = 2.718282$; $\pi = 3.141593$. Other designations are explained in comments to formulae when necessary.

1. Bremsstrahlung

We use differential cross section for bremsstrahlung as parametrized by Yu. M. Andreev, L. B. Bezrukov and E. V. Bugaev in Ref. [36] as a basic parametrization:

$$\begin{aligned} \frac{d\sigma^\gamma}{dv}(E, v) &= \alpha \left(2r_e Z \frac{m_e}{m_\mu} \right)^2 \frac{1}{v} \left[(2 - 2v + v^2) \Psi_1(q_{\min}, Z) - \frac{2}{3}(1 - v) \Psi_2(q_{\min}, Z) \right], \\ \Psi_{1,2}(q_{\min}, Z) &= \Psi_{1,2}^0(q_{\min}, Z) - \Delta_{1,2}(q_{\min}, Z), \\ \Psi_1^0(q_{\min}, Z) &= \frac{1}{2} \left(1 + \ln \frac{m_\mu^2 a_1^2}{1 + x_1^2} \right) - x_1 \arctan \frac{1}{x_1} + \frac{1}{Z} \left[\frac{1}{2} \left(1 + \ln \frac{m_\mu^2 a_2^2}{1 + x_2^2} \right) - x_2 \arctan \frac{1}{x_2} \right], \\ \Psi_2^0(q_{\min}, Z) &= \frac{1}{2} \left(\frac{2}{3} + \ln \frac{m_\mu^2 a_1^2}{1 + x_1^2} \right) + 2x_1^2 \left(1 - x_1 \arctan \frac{1}{x_1} + \frac{3}{4} \ln \frac{x_1^2}{1 + x_1^2} \right) \\ &+ \frac{1}{Z} \left[\frac{1}{2} \left(\frac{2}{3} + \ln \frac{m_\mu^2 a_2^2}{1 + x_2^2} \right) + 2x_2^2 \left(1 - x_2 \arctan \frac{1}{x_2} + \frac{3}{4} \ln \frac{x_2^2}{1 + x_2^2} \right) \right], \\ \Delta_1(q_{\min}, Z \neq 1) &= \ln \frac{m_\mu}{q_c} + \frac{\zeta}{2} \ln \frac{\zeta + 1}{\zeta - 1}, \\ \Delta_2(q_{\min}, Z \neq 1) &= \ln \frac{m_\mu}{q_c} + \frac{\zeta}{4} (3 - \zeta^2) \ln \frac{\zeta + 1}{\zeta - 1} + \frac{2m_\mu^2}{q_c^2}, \\ \Delta_{1,2}(q_{\min}, Z = 1) &= 0, \\ q_{\min} &= \frac{m_\mu^2 v}{2E(1 - v)}, \quad x_i = a_i q_{\min}, \end{aligned}$$

$$a_1 = \frac{111.7}{Z^{1/3} m_e}, \quad a_2 = \frac{724.2}{Z^{2/3} m_e}, \quad \zeta = \sqrt{1 + \frac{4m_\mu^2}{q_c^2}}, \quad q_c = \frac{1.9m_\mu}{Z^{1/3}}.$$

Integration limits for bremsstrahlung in Eqs. (2.3), (2.4), (2.6) and (3.3) are

$$v_{\min}^\gamma = 0, \quad v_{\max}^\gamma = 1 - \frac{3}{4} \sqrt{e} (m_\mu/E) Z^{1/3}.$$

Note that this parametrization does not take into account contribution from e -diagrams for bremsstrahlung when γ -quantum is emitted by atomic electrons which are knocked on by recoil (Ref. [37]). Corresponding corrections are done in parametrizations for knock-on electron production (see Sec. A 4) according to Ref. [38]. Optionally, differential cross section for muon bremsstrahlung can be also calculated in MUM according to parametrization given by S. R. Kelner, R. P. Kokoulin, and A. A. Petrukhin (Ref. [37,38]).

2. Photonuclear interaction

We use parametrization for the photonuclear interaction of muon proposed by L. B. Bezrukov and E. V. Bugaev (Ref. [39]):

$$\frac{d\sigma^{pn}}{dv} = \frac{\alpha}{8\pi} A\sigma_{\gamma N} v \left\{ H(v) \ln \left(1 + \frac{m_2^2}{t} \right) - \frac{2m_\mu^2}{t} \left[1 - \frac{0.25m_2^2}{t} \ln \left(1 + \frac{t}{m_2^2} \right) \right] \right. \\ \left. + G(z) \left[H(v) \left(\ln \left(1 + \frac{m_1^2}{t} \right) - \frac{m_1^2}{m_1^2 + t} \right) - \frac{2m_\mu^2}{t} \left(1 - \frac{0.25m_1^2}{m_1^2 + t} \right) \right] \right\},$$

$$H(v) = 1 - \frac{2}{v} + \frac{2}{v^2},$$

$$G(z) = \frac{9}{z} \left[\frac{1}{2} + \frac{(1+z)e^{-z} - 1}{z^2} \right] \quad (Z \neq 1),$$

$$G(z) = 3 \quad (Z = 1),$$

$$z = 0.00282A^{1/3}\sigma_{\gamma N}, \quad t = \frac{m_\mu^2 v^2}{1-v}, \quad m_1^2 = 0.54 \text{ GeV}^2, \quad m_2^2 = 1.80 \text{ GeV}^2.$$

Total cross section for absorption of a real photon of energy $\nu = s/2m_N = vE$ by a nucleon, $\sigma_{\gamma N}$, can be calculated in the MUM code optionally according to either parametrization from Ref [39] (basic):

$$\sigma_{\gamma N} = [114.3 + 1.647 \ln^2(0.0213 \nu)] \mu b,$$

or by recent ZEUS parametrization (Ref. [40]):

$$\sigma_{\gamma N} = (63.5 s^{0.097} + 145 s^{-0.5}) \mu b,$$

where s and ν are expressed in GeV^2 and GeV , correspondingly.

Parametrization (Ref. [39]) is valid for $\nu > 1 \text{ GeV}$, so we use values $v_{min}^{pn} = 0.8/E(\text{GeV})$ and $v_{max}^{pn} = 1$ as integration limits in Eqs. (2.3), (2.4), (2.6) and (3.3). Note that results of integration were tested to be almost insensitive to the lower limit in a wide range $0.2/E(\text{GeV}) \leq v_{min}^{pn} \leq 1.5/E(\text{GeV})$.

3. Direct electron-positron pair production

Cross section for direct e^+e^- -pair production is used in MUM as parametrized by R. P. Kokoulin and A. A. Petrukhin (Refs. [38,41,42]):

$$\frac{d\sigma^{e^+e^-}}{dv}(E, v) = \alpha^2 \frac{2}{3\pi} r_e^2 Z(Z + \zeta(Z)) \frac{1-v}{v} \int_{\rho} \left[\Phi_e + (m_e/m_\mu)^2 \Phi_\mu \right] d\rho,$$

$$\Phi_e = \left\{ [(2 + \rho^2)(1 + \beta) + \xi(3 + \rho^2)] \ln \left(1 + \frac{1}{\xi} \right) + \frac{1 - \rho^2 - \beta}{1 + \xi} - (3 + \rho^2) \right\} L_e,$$

$$\Phi_\mu = \left\{ \left[(1 + \rho^2) \left(1 + \frac{3}{2}\beta \right) - \frac{1}{\xi} (1 - \rho^2)(1 + 2\beta) \right] \ln(1 + \xi) + \frac{\xi(1 - \rho^2 - \beta)}{1 + \xi} + (1 - \rho^2)(1 + 2\beta) \right\} L_\mu,$$

$$L_e = \ln \left[\frac{R Z^{-1/3} \sqrt{(1 + \xi)(1 + Y_e)}}{1 + \frac{2m_e \sqrt{e} R Z^{-1/3} (1 + \xi)(1 + Y_e)}{E v (1 - \rho^2)}} \right] - \frac{1}{2} \ln \left[1 + \left(\frac{3}{2} \frac{m_e}{m_\mu} Z^{1/3} \right)^2 (1 + \xi)(1 + Y_e) \right],$$

$$L_\mu = \ln \left[\frac{\frac{2}{3} \frac{m_\mu}{m_e} R Z^{-2/3}}{1 + \frac{2m_e \sqrt{e} R Z^{-1/3} (1 + \xi) (1 + Y_e)}{E v (1 - \rho^2)}} \right],$$

$$Y_e = \frac{5 - \rho^2 + 4\beta (1 + \rho^2)}{2(1 + 3\beta) \ln(3 + 1/\xi) - \rho^2 - 2\beta(2 - \rho^2)},$$

$$Y_\mu = \frac{4 + \rho^2 + 3\beta (1 + \rho^2)}{(1 + \rho^2) \left(\frac{3}{2} + 2\beta \right) \ln(3 + \xi) + 1 - \frac{3}{2} \rho^2},$$

$$\beta = \frac{v^2}{2(1 - v)}, \quad \xi = \left(\frac{m_\mu v}{2m_e} \right)^2 \frac{(1 - \rho^2)}{(1 - v)}.$$

Here $\rho = (\epsilon^+ - \epsilon^-)/(\epsilon^+ + \epsilon^-)$ is the assymetry coefficient of the energy distribution of e^+e^- -pair, ϵ^+ and ϵ^- are positron and electron energies, correspondongly. Limits for integration over ρ are determined by:

$$0 \leq |\rho| \leq \left(1 - \frac{6m_\mu^2}{E^2(1 - v)} \right) \sqrt{1 - \frac{4m_e}{Ev}}.$$

R is a parameter determined by the value of radiation logarithm ($R = 183$ for Thomas-Fermi model and slightly depends upon Z for Hartrey-Fock model). Its values are taken from Ref. [43], where R has been calculated for different atoms according to Hartrey-Fock model. $\zeta(Z) \approx 1$ takes into account the pair production in collisions with electrons. Values from $\zeta(Z)$ are computed according to Refs. [38,42]. Integration limits for $j = e^+e^-$ in Eqs. (2.3), (2.4), (2.6) and (3.3) are

$$v_{min}^{e^+e^-} = \frac{4m_e}{E}, \quad v_{max}^{e^+e^-} = 1 - \frac{3}{4} \sqrt{e} (m_\mu/E) Z^{1/3}.$$

4. Knock-on electron production

Cross section for knock-on electron production is parametrized in the MUM code as follows:

$$\frac{d\sigma^\delta}{dv}(E, v) = 2\pi r_e^2 Z \frac{m_e}{E} \left(\frac{1}{v^2} - \frac{1}{v} \frac{E}{v_{max}^\delta} + \frac{1}{2} \right) (1 + \Delta_{e\gamma}(E, v)),$$

$$v_{max}^\delta = \frac{2m_e E}{m_\mu^2 + 2m_e E}.$$

$\Delta_{e\gamma}(E, v)$ represents the correction which takes into account e -diagrams for bremsstrahlung (Refs. [37,38]) resulting in additional recoil electrons:

$$\Delta_{e\gamma}(E, v) = \frac{\alpha}{2\pi} \ln \left(1 + \frac{2vE}{m_e} \right) \left[\ln \left(\frac{4E^2(1 - v)}{m_\mu^2} \right) - \ln \left(1 + \frac{2vE}{m_e} \right) \right],$$

value of v_{max}^δ is used also as upper integration limit in Eqs. (2.3) and (2.6) for $j = \delta$.

5. Ionization

Following Refs. [37,38] we treat in the MUM code e -diagrams for bremsstrahlung as a part of ionization process. Therefore we have to use a bit modified formula for ionization:

$$\left[\frac{dE}{dx}(E) \right]_{B-B} = \frac{K}{\beta^2} \frac{Z}{A} \rho \left[\ln \left(\frac{2m_e p^2 E_{\max}}{m_\mu^2 \bar{I}^2} \right) + \frac{W_{\max}^2}{4E^2} - 2\beta^2 - \delta \right] + \frac{N_A}{A_{eff}} \rho E \sum_{i=1}^n \left[k_i \int_0^{v_{max}^\delta} \Delta_{e\gamma}(E, v) v dv \right].$$

Here $K = 0.1535 \text{ MeV g}^{-1} \text{ cm}^2$, p is the muon momentum, $\beta = p/E$ is the muon velocity, ρ is the material density, \bar{I} is the mean ionization potential,

$$E_{\max} = (2m_e p^2) / (m_\mu^2 + m_e^2 + 2m_e E)$$

is the maximum energy transferable to an electron, δ is the density-effect correction which is treated according to Ref. [44]:

$$\delta = \theta(X - X_0) [4.6052X + a\theta(X_1 - X)(X_1 - X)^m + C],$$

where θ is the step function ($\theta(x) = 0$ at $x \leq 0$ and $\theta(x) = 1$ at $x > 0$), $X = \log_{10}(p/m_\mu)$. The values X_0 , X_1 , a , m and C depend on the material and can be found in Refs. [19,44] along with values for \bar{I} , ρ and Z/A . The first term represents Bethe-Bloch formula with corrections for density effect, the second one accounts bremsstrahlung e -diagrams, expressions for $\Delta_{e\gamma}(E, v)$ and v_{max}^δ are given in previous Sec. A 4, meaning of values A_{eff} and k_i is explained in Sec. II.

APPENDIX B: FREE PATH BETWEEN TWO MUON INTERACTIONS

For the proof of the set of equation (2.5) it is convenient to introduce the kinetic equation for a propagation of a monochromatic muon beam through a medium. With the notations used in textbooks this equation has the following view:

$$\begin{cases} \partial n(E, t) / \partial t - \partial [\beta(E) n(E, t)] / \partial E + n(E, t) / \lambda(E) = 0 \\ n(E, 0) = n_0 \delta(E - E_0) \end{cases} \quad (\text{B1})$$

Here, $n(E, t)$ is the number of muons with energy E after propagation of distance t , $\beta(E)$ is the ‘‘continuous’’ energy loss per unit path, $\lambda(E)$ is the muon mean free path before interaction of SEL type. The solution of Eq. (B1) is:

$$n(E, t) = n_0 \delta(E - \epsilon(E_0, t)) \exp \left[- \int_E^{E_0} dE' / \left(\lambda(E') \beta(E') \right) \right], \quad (\text{B2})$$

where $\epsilon(E_0, t)$ is found from the equation

$$\int_{\epsilon(E_0, t)}^{E_0} dE / \beta(E) = t. \quad (\text{B3})$$

Notice that Eq. (B2) can be rewritten as:

$$\eta(E, t) = \delta(E - \epsilon(E_0, t)) \exp \left[- \int_E^{E_0} dE' / \left(\lambda(E') \beta(E') \right) \right], \quad (\text{B4})$$

where $\eta(E, t)$ is the probability for a single muon to pass the path t without interaction of SEL type and then one can easily see that the formulas (B3) and (B4) lead to the Eqs. (2.5) after the following substitutions which are necessary for a return to the notations of Sec. II:

$$E_0 \rightarrow E_1, \quad E \rightarrow E_2, \quad \lambda(E) \rightarrow \bar{L}(E), \quad \beta(E) \rightarrow (dE(E)/dx)_{CEL}, \quad t \rightarrow L.$$

-
- [1] G. T. Zatsepin and E. D. Mikhailchi, *J. Phys. Soc. Japan*, **17**, Suppl. A – III, 356 (1962).
- [2] K. Kobayakawa, *Nuovo Cimento B* **47**, 156 (1967).
- [3] S. Hayakawa, *Cosmic Ray Physics – Nuclear and Astrophysical Aspects*, Interscience Monographs and Texts in Physics and Astronomy, Vol. XXII, edited by R. E. Marshak (University of Rochester, New York, 1969).
- [4] E. Kiraly, P. Kiraly, and J. L. Osborn, *J. Phys. A* **5**, 444 (1972).
- [5] A. Misaki and J. Nishimura, *Uchuusen-Kenkyuu*, **21**, 250 (1976).
- [6] V. I. Gurentsov, G. T. Zatsepin, and E. D. Mikhailchi, *Yad. Fiz.* **23**, 1001 (1976) [*Sov. J. Nucl. Phys.* **23**, 527 (1976)].
- [7] Y. Minorikawa, T. Kitamura, and K. Kobayakawa, *Nuovo Cimento C* **4**, 471 (1981).
- [8] E. V. Bugaev, V. A. Naumov, and S. I. Sinegovsky, *Yad. Fiz.* **41**, 383 (1985) [*Sov. J. Nucl. Phys.* **41**, 245 (1985)]; *Izv. Akad. Nauk SSSR. Ser. Fiz.* **49**, 1389 (1985) [*Proc. of the Acad. of Sci. of the USSR. Phys. Ser.* **49**, 146 (1985)].
- [9] D. P. Bhattacharyya, *Nuovo Cimento C* **9**, 404 (1986).
- [10] O. C. Allkofer and D. P. Bhattacharyya, *Phys. Rev. D* **34**, 1368 (1986).
- [11] V. N. Bakatanov *et al.*, *Yad. Fiz.* **55**, 2107 (1992) [*Sov. J. Nucl. Phys.* **55**, 1169 (1992)].
- [12] V. A. Naumov, S. I. Sinegovsky, and E. V. Bugaev, *Yad. Fiz.* **57** (1994) 439 [*Physics of Atomic Nuclei* **57** (1994) 412].
- [13] E. V. Bugaev *et al.*, *Phys. Rev. D* **58**, 054001 (1998); see also Report No. hep-ph/9803488 for more details and references.
- [14] P. J. Hayman, N. S. Palmer, and A. W. Wolfendale, *Proc. Roy. Soc. (London)* **A275**, 391 (1963).
- [15] J. L. Osborn, A. W. Wolfendale, and E. C. M. Young, *J. Phys. A* **1**, 55 (1968).
- [16] L. Bergamasco and P. Picchi, *Nuovo Cimento B* **3**, 134 (1971).
- [17] Yu. N. Vavilov, Yu. A. Trubkin, and V. M. Fedorov, *Yad. Fiz.* **18**, 884 (1974) [*Sov. J. Nucl. Phys.* **18**, 434 (1974)].
- [18] N. Takahashi *et al.*, *Uchuusen-Kenkyuu*, **28**, 120 (1984).
- [19] W. Lohmann, R. Kopp, and R. Voss, CERN Report No. 85-03, 1985 (unpublished); MUDEDX code was written by authors on the base of preprint.
- [20] J. N. Capdevielle *et al.*, *J. Phys. G* **11**, 565 (1985).
- [21] H. Bilokon *et al.*, *Nucl. Instrum. Methods* **A303**, 381 (1991).
- [22] P. Lipari and T. Stanev, *Phys. Rev. D* **44**, 3543 (1991).
- [23] K. Mitsui, *Phys. Rev. D* **45**, 3051 (1992).
- [24] P. Antonioli *et al.*, *Astropart. Phys.* **7**, 357 (1997), V. A. Kudryavtsev *et al.*, *Phys. Lett. B* **471**, 251 (1999).
- [25] A. A. Lagutin, P. B. Togobitsky, and A. Misaki, *Izv. Altayskogo Gos. Universiteta* **Special issue**, 93 (1998).
- [26] W. Rhode and C. Cârloganu, in *Proceedings of the Workshop on Simulation and Analysis Methods for Large Neutrino Telescopes, Zeuthen, 1998*, edited by C. Spiering (DESY Zeuthen, Zeuthen, 1998), p. 247.
- [27] Ch. Spiering and I. Sokalski (eds.), Baikal Collaboration Report No. 92/11, 1992; Baikal Collaboration, V. A. Balkanov *et al.*, *Nucl. Phys. Proc. Suppl.* **87**, 405 (2000).
- [28] S. Barwick *et al.*, Wisconsin University Report No. MAD-PH-629, 1991; E. Andres *et al.*, *Astropart. Phys.* **13**, 1 (2000).
- [29] E. Aslanides *et al.*, Report No. astro-ph/9907432, 1999; P. Amram *et al.*, *Nucl. Phys. Proc. Suppl.* **75A**, 415 (1999).
- [30] L. K. Resvanis *et al.*, *Nucl. Phys. Proc. Suppl.* **35**, 294 (1994); S. Bottai *et al.*, *Nucl. Phys. Proc. Suppl.* **85**, 153 (2000).
- [31] E. V. Bugaev, I. A. Sokalski, and S. I. Klimushin, Report No. hep-ph/0010323, 2000.
- [32] R. P. Kokoulin, A. A. Petrukhin, in *Proceedings of the 22nd International Cosmic Ray Conference, Dublin, 1991*, edited by M. Cawley *et al.* (The Dublin Institute for Advanced Studies, Dublin, 1991), Vol. **4**, p. 536; R. P. Kokoulin, *Nucl. Phys. B (Proc. Suppl.)* **70**, 475 (1999).
- [33] S. I. Klimushin, E. V. Bugaev, and I. A. Sokalski, Report No. hep-ph/0012032, 2000.
- [34] T. K. Gaisser, *Cosmic Rays and Particle Physics* (Cambridge University Press, Cambridge, 1990).
- [35] V. A. Kudryavtsev (private communication, August 2000).
- [36] L. B. Bezrukov and E. V. Bugaev, in *Proceedings of the 17th International Cosmic Ray Conference, Paris, 1981* (Section d’Astrophysique, Centre d’Études Nucléaires de Saclay, Gif-sur-Yvette, Cedex, 1981), Vol. **7**, p. 102; Yu. M. Andreev, L. B. Bezrukov, and E. V. Bugaev, *Yad. Fiz.* **57**, 2146 (1994) [*Phys. At. Nucl.* **57**, 2066 (1994)].
- [37] S. R. Kelner, R. P. Kokoulin, and A. A. Petrukhin, Moscow Engineering Physics Inst. Preprint No. 024-95, 1995; S. R. Kelner, R. P. Kokoulin, A. A. Petrukhin, *Yad. Fiz.* **60**, 576 (1997) [*Phys. At. Nucl.* **60**, 657 (1997)].
- [38] R. P. Kokoulin kindly granted us in November, 1999 routines which had been written by him to compute muon cross sections. Some part of these routines are used in the MUM code.
- [39] L. B. Bezrukov and E. V. Bugaev, *Yad. Fiz.* **32**, 1636 (1980) [*Sov. J. Nucl. Phys.* **32**, 847 (1980)]; *ibid.* **33**, 1195 (1981) [**33**, 635 (1981)].
- [40] J. Breitweg *et al.*, *Europ. Phys. J.* **C7**, 609 (1999).
- [41] R. P. Kokoulin and A. A. Petrukhin, in *Proceedings of the 11th International Cosmic Ray Conference, Budapest, 1969*, edited by T. Gémsey *et al.* [*Acta Phys. Acad. Sci. Hung.* **29**, Suppl. 4, 277 (1970)]; R. P. Kokoulin and A. A. Petrukhin, in *Proceedings of the 12th International Cosmic Ray Conference, Hobart, 1971*, edited by A. G. Fenton and K. B. Fenton

(University of Tasmania Press, Hobart, 1971), Vol. **6**, p. A 2436.

[42] S. R. Kelner, Moscow Engineering Physics Inst. Preprint No. 016-97, 1997.

[43] S. R. Kelner, R. P. Kokoulin, and A. A. Petrukhin, *Yad. Fiz.* **62**, 2042 (1999) [*Phys. Atom. Nucl.* **62**, 1894 (1999)].

[44] R. M. Sternheimer, *Phys. Rev.* **103**, 511 (1956); R. M. Sternheimer and R. F. Peierls, *Phys. Rev. B* **3**, 3681 (1971); R. M. Sternheimer, M. J. Berger, and S. M. Seltzer, *Atomic Data and Nuclear Data Tables*, **30**, 261 (1984).